frontiers in Chemistry

ORIGINAL RESEARCH
published: 21 November 2018
doi: 10.3389/fchem.2018.00555

A Porous and Conductive Graphite Nanonetwork Forming on the Surface of KCu_7S_4 for Energy Storage

Wei-Xia Shen, Jun-Min Xu, Shu-Ge Dai and Zhuang-Fei Zhang**

Key Laboratory of Material Physics of Ministry of Education, Zhengzhou University, Zhengzhou, China

A flexible all-solid-state supercapacitor is fabricated by building a layer of porous and conductive nanonetwork on the surface of KCu_7S_4 nanowires supported on the carbon fiber fabric, where the porous and conductive nanonetwork is assembled by graphite nanoparticles. This porous graphite layer plays a key role in providing ion diffusion channels to access the KCu_7S_4 through the pores for electrochemical reactions and forming electron transport pathways from the graphite network to the electronic collector of the carbon fiber fabric. This flexible supercapacitor exhibits excellent electrochemical performance with high specific capacitance of 408 F g^{-1} at a current density of 0.5 A g^{-1} and high energy density of 36 Wh kg^{-1} at a power density of 201 W kg^{-1}. Moreover, it is cost-effective, easy to scale up and environmentally friendly with high flexibility. Our investigation demonstrates that such a porous and conductive nanonetwork could be used to improve the charge storage efficiency for a wide range of electrode materials.

Keywords: flexible, porous, graphite nanonetwork, KCu_7S_4 nanowires, supercapacitor

OPEN ACCESS

Edited by:
Qiaobao Zhang,
Xiamen University, China

Reviewed by:
Aibing Chen,
Hebei University of Science and Technology, China
Haibin Sun,
Shandong University of Technology, China
Shanglong Peng,
Lanzhou University, China

****Correspondence:***
Shu-Ge Dai
shugedai@zzu.edu.cn
Zhuang-Fei Zhang
zhangzf@zzu.edu.cn

Specialty section:
This article was submitted to Nanoscience, a section of the journal Frontiers in Chemistry

Received: *27 September 2018*
Accepted: *29 October 2018*
Published: *21 November 2018*

Citation:
Shen W-X, Xu J-M, Dai S-G and Zhang Z-F (2018) A Porous and Conductive Graphite Nanonetwork Forming on the Surface of KCu_7S_4 for Energy Storage. Front. Chem. 6:555. doi: 10.3389/fchem.2018.00555

INTRODUCTION

Nowadays, it is a great challenge to develop supercapacitors (SCs) with flexibility, lightweight and high electrochemical performance. In general, the quality of the SCs strongly depends on the design of an appropriate configuration and the innovation of electrode materials (Niu et al., 2013). For the traditional electrodes in SCs, carbonaceous materials (activated carbon, graphite, carbon nanotubes, and graphene) can offer very high power density and excellent cycling ability (Niu et al., 2017; Du et al., 2018; Liu et al., 2018). However, the energy density of carbon-based materials is still too low to meet the requirement for SCs in practical applications (Lu et al., 2014; Guan et al., 2015; Wang et al., 2016; Xia et al., 2017; Dai et al., 2018). Compared with carbon-based SCs, transition-metal oxides/sulfides have attracted particular attention since they could offer much higher energy density by Faradaic reactions (Augustyn et al., 2014; Simon et al., 2014; Dai et al., 2017; Qu et al., 2017; Xu et al., 2017; Zhang et al., 2018a). However, they usually suffer from low electrical conductivity, poor rate performance and limited cycling stability (Liu et al., 2010; Xia et al., 2014; Dai et al., 2016a; Jiang et al., 2018). To overcome the accumulation of produced charges on the surface of pseudo-capacitor material which could not successfully reach electron collector, the design of hybrid structure electrodes is an efficient way for SCs with excellent electrochemical performance (Chang et al., 2012; Qu et al., 2018a,b; Zhang et al., 2018b; Zheng et al., 2018a).

Recently, transition-metal oxides are emerging as promising electrode materials for energy storage devices, such as RuO_2, MnO_2, NiO, Fe_2O_3, WO_3, V_2O_5 (Xue et al., 2011; Dang et al., 2018; Zheng et al., 2018b). Among them, manganese oxides have been widely studied as electrode

materials for SCs due to their high theoretical capacitance, low-cost, environmentally friendliness and natural abundance. The α-MnO_2 is constructed from double chains of octahedral [MnO_6] structure with 2 × 2 and 1 × 1 tunnels, which is beneficial for Li^+ transportation (Park et al., 2007; Reddy et al., 2009). However, its actual capability is often much lower than the theoretical value owing to its low electronic conductivity. Besides, it also displays poor capacity retention and large volume change during Li^+ insertion/extraction (Wang et al., 2014a). Similar to the crystal structure of α-MnO_2, the KCu_7S_4 has one-dimensional double tunnels along c axis, which is composed of a three-dimensional Cu-S framework that contains pseudo-one-dimensional channels in which K ions reside in the channels (Hwu et al., 1998; Dai et al., 2013, 2014a). Compared with a-MnO_2, the KCu_7S_4 exhibits greater conductivity and capacity retention, which is one of the most promising electrode materials for energy storage (Dai et al., 2013, 2014a; Guo et al., 2016). Moreover, the KCu_7S_4 has significant advantages, such as large surface area, low-cost, easy synthesis, and environmentally friendliness. To improve the performance, many researchers have focused on the surface modification of the micro/nano electrode materials, such as Au nanoparticles coated WO_{3-x} NWs (Lu et al., 2012), graphene quantum dots coated VO_2 arrays (Chao et al., 2015), CNTs decorated MoO_3 (Yang et al., 2014a). It is an effective way to enhance the electrical conductivity of the electrode materials, which improves the ion diffusion kinetics and electron transport by coating of nanostructured conductive layer. Herein, we design a porous and conductive nanonetwork by coating graphite nanoparticles on the surface of KCu_7S_4 nanowires, which not only ensures the multichannel diffusion of electrolyte ions insert the KCu_7S_4 material, but also improves the electron transportation. It is no doubt that this porous and conductive nanonetwork structure will attract more attention in the design of the electrodes for SCs.

Currently, the fabricated electrodes based on KCu_7S_4 materials are too rigid and bulky, which could not meet the practical requirements for flexible and wearable electronic devices (Dai et al., 2014b, 2015). Therefore, the exploration of flexible, lightweight, or even wearable SCs based on the KCu_7S_4 materials will be interesting work. Recently, carbon fiber fabric (CFF) attracts many people's interest because of its unique characteristics, such as low corrosion resistance, low thermal expansion coefficient and excellent flexibility. Moreover, all-solid-state supercapacitors based on CFF can be easily bent or twisted, which could meet the requirements for flexible and wearable electronic devices (Yuan et al., 2012).

In this work, we report a highly flexible all-solid-state SC based on a layer of porous and conductive graphite nanonetwork coated on the surface of KCu_7S_4 nanowires, which is supported on a carbon fiber fabric (GN/KCu_7S_4/CFF). The GN/KCu_7S_4/CFF SC exhibits great electrochemical performance with the highest specific capacitance of 408 F g^{-1} and the highest energy density of 36 Wh kg^{-1} at a power density of 201 W kg^{-1}. The enhanced capacity attributed to the porous and conductive nanonetwork on the surface of the KCu_7S_4 nanowires, which provides rich ion diffusion channels to access the KCu_7S_4, and shortens the electron transmission paths through the graphite network to

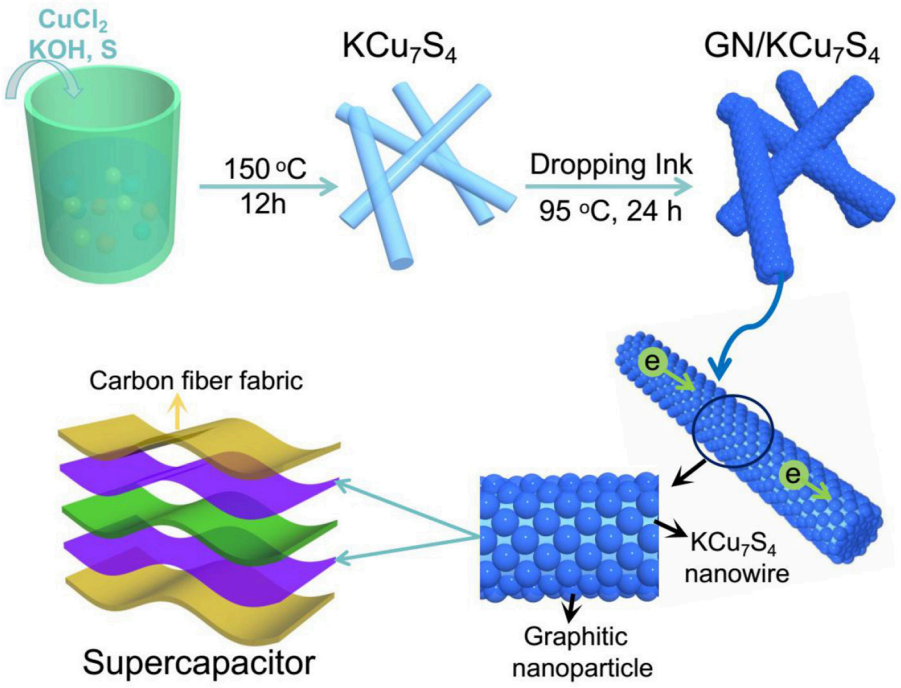

FIGURE 1 | Schematic diagram of preparing of GN/KCu_7S_4 nanowires and the fabrication of flexible GN/KCu_7S_4/CFF SC.

the electronic collector of CFF. This work demonstrates that the porous and highly conductive graphite nanonetwork could be used to improve the charge storage for a wide range of electrode materials, revealing a promising application in the flexible energy-storage devices.

EXPERIMENTAL SECTION

Preparation of GN/KCu_7S_4/CFF Electrode

Carbon fiber fabric (Shanghai Lishuo Composite Material Technology Company) and the graphite ink (from Hero, Shanghai Ink Factory in China) were used as purchased. First, 1 mmol of $CuCl_2 \cdot 2H_2O$, 2.5 mmol of S, and 53 mmol of KOH were dissolved in deionized water (10 mL) in the Teflon containers, followed by addition of 2 mL of hydrazine monohydrate. Then the mixed solution was retained at 150°C for 12 h. After cooled down to room temperature, the product was rinsed with ultrapure water, and dried under vacuum at 60°C overnight. The GN/KCu_7S_4/CFF was made as follows: 100 mg of as-prepared KCu_7S_4 nanowires was first dispersed in ultrapure water (10 mL). Then the graphite ink was dropped into the KCu_7S_4 solution (the ratio of ink to water is 1:10) under magnetic stirring for 24 h at 95°C. Finally, the mixture was filtered on the CFF to obtain the GN/KCu_7S_4/CFF, where free nanoparticles were removed through the pores of the CFF. The product was put into oven for 2 h at 60°C for drying.

Fabrication of All-Solid-State Supercapacitor

The separator (Whatman 8 μm filter paper) covered with a layer of PVA-LiCl gel as a solid electrolyte on both sides and, sandwiched between the two pieces of the GN/KCu_7S_4/CFF electrodes to form a two electrode device. The detailed fabrication process of the electrode was reported in our previous work (Javed et al., 2015). Here, the mass loading on the carbon fiber fabric is about 2 mg cm^{-2} and the working area of each electrode is 4 cm × 1.5 cm.

Characterization and the Electrochemical Measurements

The morphology, chemical composition, and the structure of the products were observed by X-ray diffraction (XRD) analysis (XRD, PA National X′ Pert Pro with Cu Kα radiation). The microstructure and morphology of NC nanomaterials were characterized using field emission scanning electron microscopy (Zeiss, sigma300) and high-resolution transmission electron microscopy (HRTEM, JEOL, JEM-2100) with energy dispersive X-ray spectrometry (EDS). The nitrogen adsorption-desorption isotherm measurement of the sample was performed using a ASAP2420-4MP. The specific surface area was obtained by the Brunauer-Emmett-Teller (BET) method. The electrochemical measurement was conducted with an

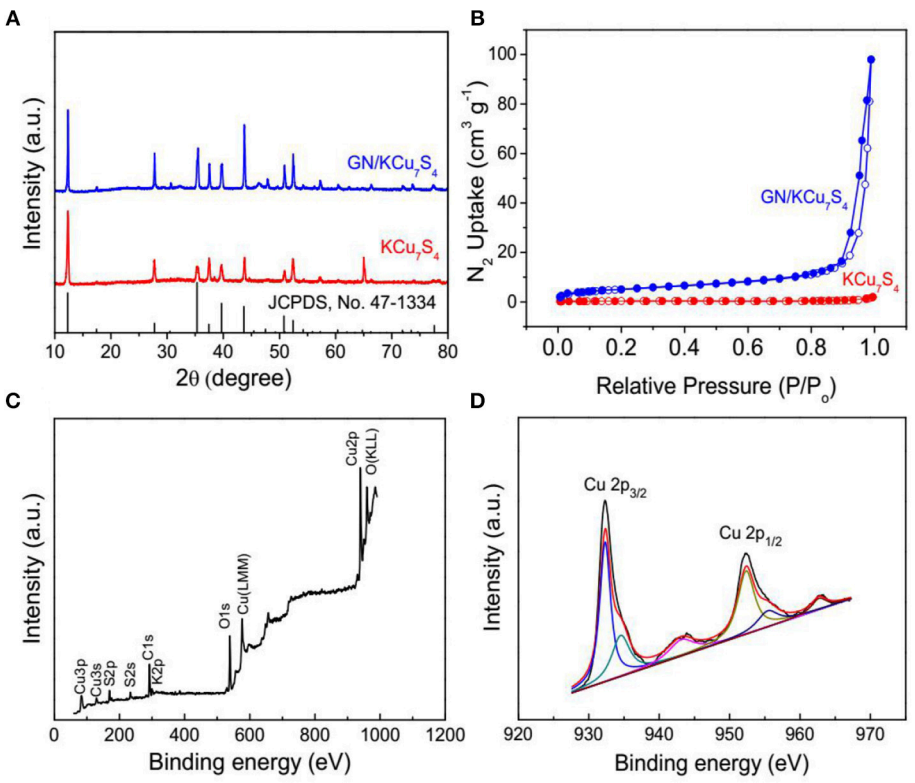

FIGURE 2 | (A) XRD patterns of KCu_7S_4 and GN/KCu_7S_4 samples. **(B)** The nitrogen adsorption-desorption isotherms of as-prepared KCu_7S_4 and GN/KCu_7S_4 samples. **(C)** XPS spectra of as-prepared KCu_7S_4 sample, and **(D)** Cu 2p XPS spectra of as-prepared KCu_7S_4 sample.

electrochemical workstation (CHI 760D). X-ray photoelectron spectrometer (XPS) analysis was performed on an ESCA Lab MKII using Mg Ka as the exciting source.

RESULTS AND DISCUSSION

Figure 1 shows the schematic diagram of preparing of GN/KCu_7S_4 nanowires and the fabrication of flexible GN/KCu_7S_4/CFF SC, respectively. The X-ray diffraction of KCu_7S_4 and GN/KCu_7S_4 nanowires indicate that the samples are well crystallized (**Figure 2A**). All the diffraction peaks can be unambiguously assigned to tetragonal KCu_7S_4 structure. To understand the porosity and surface area of as-prepared samples, N_2 adsorption-desorption isotherms of KCu_7S_4 and GN/KCu_7S_4 conducted at 77.350 K were investigated and are displayed in **Figure 2B**. Through BET analysis, the surface areas of KCu_7S_4 and GN/KCu_7S_4 samples were identified as 1 m^2g^{-1} and 18.6 m^2g^{-1}, respectively. To identify the chemical states of Cu element in the samples, the XPS survey spectrum of the KCu_7S_4 nanowires and high-resolution XPS spectrum of Cu 2p were also conducted (**Figures 2C,D**). It consists of two binding energy of Cu $2p_{3/2}$ and Cu $2p_{1/2}$ peaks at 932.3 and 952.2 eV, respectively, which are in agreement with the previous reports (Colleen and McShane, 2012; Wang et al., 2013). Scanning electron microscopy (SEM) images of as-prepared KCu_7S_4 and GN/KCu_7S_4 samples are shown in **Figure 3**, **Figure S1**. The KCu_7S_4 nanowires have a diameter of 200–500 nm and length up to 110 μm. The enlarged image (**Figure 3b**) of GN/KCu_7S_4 nanowires clearly indicates that the KCu_7S_4 nanowires were coated with graphite nanoparticles with high homogeneity. For further confirmation, the EDS of a single GN/KCu_7S_4 nanowire is presented in **Figure 3c**, revealing the main compositions of C, K, Cu, and S. This good composite nanostructure was also further confirmed by transmission electron microscopy (TEM) analysis, as shown in **Figures 3d,e**. In order to explore the composition of the graphite ink and GN/KCu_7S_4, we also carried out a Raman test and the results are presented in **Figure 3f**, **Figure S2**. The G and D peaks are clearly observed at 1355 cm^{-1} (attributed to the disordered carbonaceous component) and 1585 cm^{-1} (attributed to the ordered graphitic component), respectively, which exhibits that the active component in graphite ink is mainly graphitic carbon (Cai et al., 2012; Dai et al., 2014c). The peak at 472 cm^{-1} corresponds to the KCu_7S_4 (**Figure S2**). Moreover, the TEM-EDX elemental mapping of the GN/KCu_7S_4 reveals a relatively uniform distribution of K, Cu, S, and C elements over the nanowire, which indicates the KCu_7S_4 nanowires were well wrapped by the graphite nanoparticles. Owing to the strong adhesion of the graphite nanoparticles bounded together to form a porous nanonetwork structure on the surface of the KCu_7S_4 nanowires, the nanonetwork can provide efficient ion diffusion multichannels to access the KCu_7S_4 and shorten the electron transport pathways to

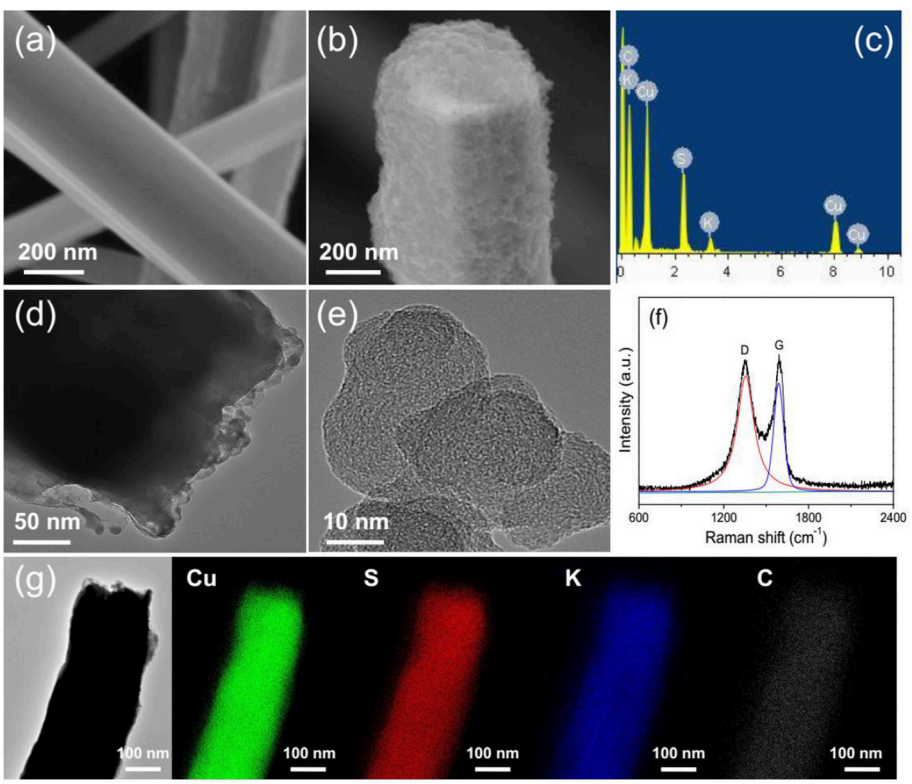

FIGURE 3 | (a) SEM image of the KCu_7S_4 nanowires. **(b)** SEM images of the GN/KCu_7S_4 nanowires. **(c)** EDS of a single GN/KCu_7S_4 nanowire. **(d)** TEM images of the GN/KCu_7S_4 nanowires and **(e)** graphite nanoparticle. **(f)** Raman spectrum of the graphite ink. **(g)** TEM-EDX mapping images of GN/KCu_7S_4 nanowire.

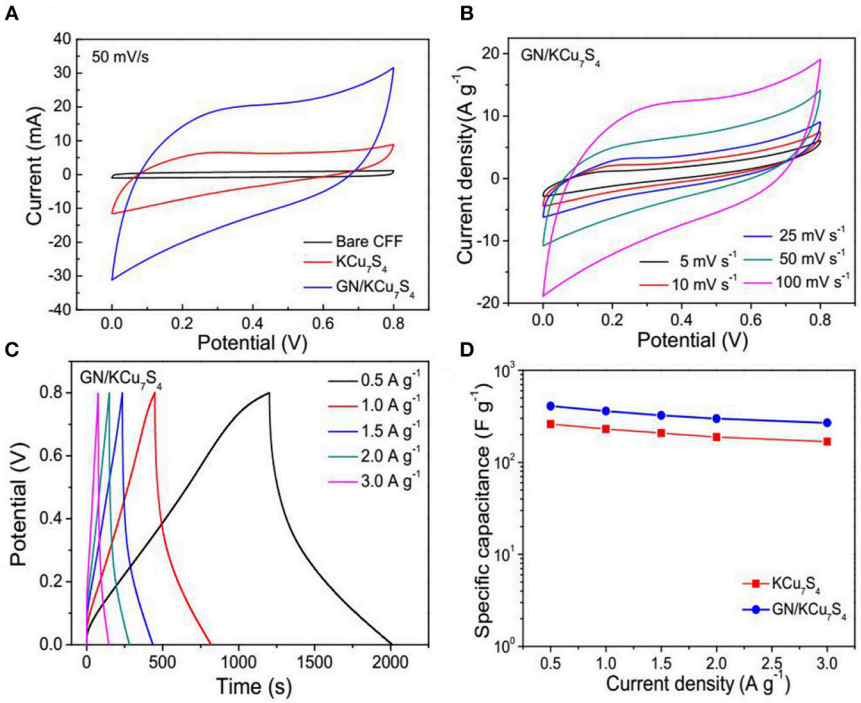

FIGURE 4 | (A) CV curves of bare CFF, KCu_7S_4 /CFF and GN/KCu_7S_4/CFF SCs at a scan rate of 100 mV/s. **(B)** CV curves of the GN/KCu_7S_4/CFF SC at different scan rates. **(C)** Galvanostatic charge-discharge curves of the GN/KCu_7S_4/CFF SC at various current densities. **(D)** Specific capacitances of the KCu_7S_4 /CFF and GN/KCu_7S_4/CFF SCs at different current densities.

the electronic collector of CFF (Fu et al., 2012; Dai et al., 2016b).

The electrochemical performance of the supercapacitors based on the KCu_7S_4/CFF and GN/KCu_7S_4/CFF are characterized by using cyclic voltammetry (CV), galvanostatic charge-discharge (GCD) cycling and electrochemical impedance spectroscopy (EIS), respectively. **Figure 4A** shows the CV curves of the bare CFF, KCu_7S_4, and /GN/KCu_7S_4/CFF based SCs at a constant scan rate of 100 m V/s. It is note that the GN/KCu_7S_4/CFF SC shows a higher capacitance behavior as compared with others. **Figure 4B** exhibits the CV curves of the GN/KCu_7S_4/CFF SC at different scan rates in potential windows from 0 to 0.8 V. All the CV curves exhibit an approximate shape with slight variations, even at a scan rate of 100 m V/s, revealing the good capacitive behavior of the GN/KCu_7S_4/CFF electrodes. The CV curves of KCu_7S_4 SC at different scan rates were also collected and is shown in **Figure S3A**. The galvanostatic charge-discharge curves of the GN/KCu_7S_4/CFF SC at various current densities in potential windows from 0 to 0.8 V (**Figure 4C**) exhibit good linear and almost symmetrical voltage-time profiles with small *IR* drops, indicating high output power of the GN/KCu_7S_4/CFF SC. The corresponding galvanostatic charge-discharge curves of the KCu_7S_4/CFF SC at various current densities are shown in **Figure S3B**. The specific capacitances of KCu_7S_4/CFF and GN/KCu_7S_4/CFF SCs were calculated by the mass loading of KCu_7S_4 and GN/KCu_7S_4 NWs on the CFFs, respectively, and the results are shown in **Figure 4D**. The maximum specific capacitance of 408 F g^{-1} at a current density of 0.5 A g^{-1} for the GN/KCu_7S_4/CFF SC was calculated, which is two times higher than that of KCu_7S_4/CFF SC (167 F g^{-1}). The enhanced electrochemical performance of the GN/KCu_7S_4/CFF electrodes benefits from the following facts. First, the nanonetwork assembled by the graphite nanoparticles on the surface of KCu_7S_4 nanowires improves the conductivity of the KCu_7S_4 nanowires, which greatly increases the electron transmission rate. Secondly, these nanoparticles aggregated together to form a porous structure on the surface of the KCu_7S_4 nanowires, which provides rich channels for ions to access to electroactive sites for fast and reversible redox reactions (Guan et al., 2015). The specific capacitance of the GN/KCu_7S_4/CFF SC in this work is higher than that of the previously reported for the hybrid SCs, such as 80.8 F g^{-1} at 0.5 A g^{-1} for the GNS/αMWCNT@PDAA SC (Sun et al., 2015), 56 F g^{-1} at 0.58 A g^{-1} for the MSCS-O SC (Kim et al., 2015), 156 F g^{-1} at 0.5 A g^{-1} for the PG-paper SC (Shu et al., 2015), and 189 F g^{-1} at 0.5 A g^{-1} for the $FeMnO_3$/RGO SC (Li et al., 2014). These results indicate that the electrochemical performance of the KCu_7S_4 nanowires is improved by the successful coating of the graphite nanoparticles and this method can also be applied for other metal sulfides.

The EIS is measured in the frequency from 100 kHz to 1 Hz, and the Nyquist impedance plots of the KCu_7S_4/CFF and GN/KCu_7S_4/CFF SCs are shown in **Figure S4A**. In the high frequency range, the intercepts of the Nyquist curves on the real axis are about 2.43 Ω and 2.18 Ω for the

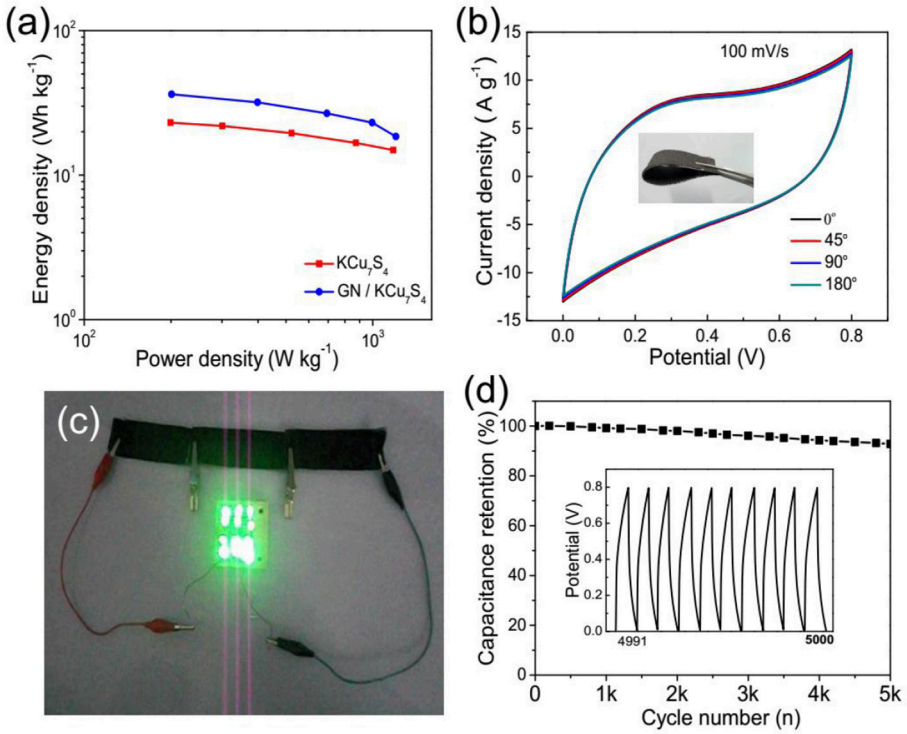

FIGURE 5 | (a) Ragone plots of the prepared KCu_7S_4 /CFF and GN/KCu_7S_4/CFF SCs. **(b)** CV curves of the GN/KCu_7S_4/CFF SC at different curvatures of 0^o, 45^o, 90^o, and 180^o. **(c)** Optical photograph of 12 commercialized LEDs lighted by three GN/KCu_7S_4/CFF SCs connected in series. **(d)** Cycling life of the GN/KCu_7S_4/CFF SC.

KCu_7S_4/CFF and GN/KCu_7S_4/CFF SCs, respectively, indicating better conductivity after coating the graphite nanoparticles. A smaller arc is observed for the GN/KCu_7S_4/CFF SC, which demonstrates an enhanced ion accessibility of the GN/KCu_7S_4 nanowires compared with that of KCu_7S_4 nanowires, due to the highly porous network structure. The Nyquist plots show almost a vertical line in the low frequency, indicating an excellent capacitive behavior of SC. To obtain more detailed information, the dependence of the phase angle on the frequency for the KCu_7S_4/CFF and GN/KCu_7S_4/CFF SCs are shown in **Figure S4B**. The relaxation time $\tau_0(_{\tau_0=1/f_0})$ evaluated from the frequency at 45° impedance phase angle is 0.09 s for the GN/KCu_7S_4/CFF, which is shorter than that of the KCu_7S_4/CFF (0.14 s), revealing larger power response of the GN/KCu_7S_4/CFF SC (Liu et al., 2015).

Energy density (E) and power density (P) are two important parameters for evaluating the electrochemical performance of SCs (Lu et al., 2012). The energy density viruses the average power density is calculated from the charge-discharge curves (**Figure 5a**), which are estimated according to the following equations (Dai et al., 2014c).

$$E = \frac{CV^2}{2M} \quad (1)$$

$$P = \frac{E}{t} \quad (2)$$

where C, M, V, *and* t are the total capacitance of the device, effective mass of the electrode, voltage and the discharge time, respectively. The highest energy density of the GN/KCu_7S_4/CFF SC is 36 Wh kg^{-1} at a power density of 201 W kg^{-1}, which is higher than that of KCu_7S_4/CFF SC with the energy density of 14 Wh kg^{-1} at a power density of 190 W kg^{-1}. The maximum energy density of the GN/KCu_7S_4/CFF SC is higher than those previously reported, such as 6.3 Wh kg^{-1} for the WL-MnO_2 SC (Yang et al., 2014b), 17 Wh kg^{-1} for the $MnFe_2O_4$/graphene/polyaniline SC (Sankar and Selvan, 2015), 12.3 Wh kg^{-1} for the MnO_2@KCu_7S_4 hybrid SC (Wang et al., 2014c), 22 Wh kg^{-1} for the CoOH//VN SC (Wang et al., 2014b), and 1.46 Wh kg^{-1} for the Al-doped α-MnO_2 SC (Hu et al., 2015).

For efficient energy storage devices, flexible, lightweight, and portable electronic devices are desired in practical applications. **Figure 5b** displays the high flexibility of as-prepared GN/KCu_7S_4/CFF SC, and it can be folded and twisted without destroying its physical structure. Moreover, the CV curves of the GN/KCu_7S_4/CFF SC hardly change under different bending angles, indicating its good flexibility. For practical applications, it is necessary to connect SCs in series and/or in parallel to increase the operating voltage and/or current in some situations (Yuan et al., 2013). **Figure 5c** shows three GN/KCu_7S_4/CFF SCs connected in series can light 12 commercial light-emitting diodes (LEDs) for about 5 min after charging at 12 A g^{-1} for 50 s (for detailed information,

see **Supporting Information**). The excellent properties of the flexible GN/KCu_7S_4/CFF SC reveal a potential application in superior storage devices. In addition, the GN/KCu_7S_4/CFF SC exhibits a long-term cycling stability between 0 and 0.8 V at a current density of 2 A g^{-1} and keeps 90% of its initial capacitance after 5,000 cycles (**Figure 5d**), revealing its good cycling life.

CONCLUSION

In summary, we have successfully designed a porous and highly conductive nanonetwork structure electrode by coating graphite nanoparticles on the surface of the KCu_7S_4 nanowires. Such a porous nanonetwork not only facilitates the diffusion of the electrolyte ions into the pseudocapacitive material, but also improved the electron transmission, which greatly enhance the charge storage efficiency. Moreover, a highly flexible all-solid-state hybrid SC based on the GN/KCu_7S_4 nanowires is fabricated, which shows excellent electrochemical properties, including the high specific capacitance (408 F g^{-1}), high energy density (36 Wh kg^{-1}), and good cyclic stability. All the results indicate that such porous and highly conductive nanonetwork forming on nanostructured pseudocapacitive materials could improve the charge storage efficiency of supercapacitors.

AUTHOR CONTRIBUTIONS

W-XS carried out the material preparation, electrochemical test, and analyzed the XRD, SEM, TEM, and Raman analysis. S-GD wrote the paper and J-MX discussed the results and revised the manuscript. Z-FZ attained the main financial support for the research and supervised all the experiments.

ACKNOWLEDGMENTS

This work is supported by the National Natural Science Foundation of China (Grant No. 21805247, Grant No. 11704340), the China Postdoctoral Science Foundation (Grant No. 2018M630831), the Youth Teacher Start Fund of Zhengzhou University (Grant No. 11704340, Grant No. 32210813).

SUPPLEMENTARY MATERIAL

The Supplementary Material for this article can be found online at: https://www.frontiersin.org/articles/10.3389/fchem.2018.00555/full#supplementary-material

REFERENCES

Augustyn, V., Simon, P., and Dunn, B. (2014). Pseudocapacitive oxide materials for high-rate electrochemical energy storage. *Energy Environ. Sci.* 7, 1597–1614. doi: 10.1039/c3ee44164d

Cai, X., Lv, Z., Wu, H., Hou, S., and Zou, D. (2012). Direct application of commercial fountain pen ink to efficient dye-sensitized solar cells. *J. Mater. Chem. A* 22, 9639–9644. doi: 10.1039/c2jm16265b

Chang, C. H., Huang, T. C., Peng, C. W., Yeh, T. Z., Lu, H., Hung, W. I., et al. (2012). Novel anticorrosion coatings prepared from polyaniline/graphene composites. *Carbon* 50, 5044–5051. doi: 10.1016/j.carbon.2012.06.043

Chao, D., Zhu, C., Xia, X., Liu, J., Zhang, X., Wang, J., et al. (2015). Graphene quantum dots coated VO_2 arrays for highly durable electrodes for Li and Na ion batteries. *Nano Lett.* 15, 565–573. doi: 10.1021/nl504038s

Colleen, M., and McShane, K. C. S. (2012). Junction studies on electrochemically fabricated p-n Cu_2O homojunction solar cells for efficiency enhancement. *Phys. Chem. Chem. Phys.* 14, 6112–6118. doi: 10.1039/c2cp40502d

Dai, S., Guo, H., Wang, M., Liu, J., and Wang, G. (2014c). A flexible micro-supercapacitor based on a pen ink-carbon fiber thread. *J. Mater. Chem. A* 2, 19665–19669. doi: 10.1039/c4ta03442b

Dai, S., Liu, J. L., Wang, C. S., Wang, X., Xi,. Y., Wei, D. P., et al. (2016a). Hierarchical porous nanostructures of manganese(III) oxyhydroxide for all-solid-state flexible supercapacitors. *Energy Technol.* 4, 1450–1454. doi: 10.1002/ente.201600212

Dai, S., Xi, Y., Hu, C., Hu, B., Yue, X., Cheng, L., et al. (2014b). C@KCu_7S_4 microstructure for solid-state supercapacitors. *RSC Adv.* 4, 40542–40545. doi: 10.1039/c4ra04893h

Dai, S., Xi, Y., Hu, C., Liu, J., Zhang, K., Yue, X., et al. (2013). KCu_7S_4 nanowires and the Mn/KCu_7S_4 nanostructure for solid-state supercapacitors. *J. Mater. Chem. A* 1, 15530–15534. doi: 10.1039/c3ta12839c

Dai, S., Xi, Y., Hu, C., Yue, X., Cheng, L., and Wang, G. (2014a). Different proportions of C/KCu_7S_4 hybrid structure for high-performance supercapacitors. *J. Power Sources* 263, 175–180. doi: 10.1016/j.jpowsour.2014.03.138

Dai, S., Xi, Y., Hu, C., Yue, X., Cheng, L., and Wang, G. (2015). MnO_2@KCu_7S_4 NWs hybrid compositions for high-power all-solid-state supercapacitor. *J. Power Sources* 274, 477–482. doi: 10.1016/j.jpowsour.2014.10.075

Dai, S., Xu, W., Xi, Y., Wang, M., Gu, X., Guo, D., et al. (2016b). Charge storage in KCu_7S_4 as redox active material for a flexible all-solid-state supercapacitor. *Nano Energy* 19, 363–372. doi: 10.1016/j.nanoen.2015.11.025

Dai, S. G., Liu, Z., Zhao, B., Zeng, J. H., Hu, H., Zhang, Q. B., et al. (2018). A high-performance supercapacitor electrode based on N-doped porous graphene. *J. Power Sources* 387, 43–48. doi: 10.1016/j.jpowsour.2018.03.055

Dai, S. G., Zhao, B., Qu, C., Chen, D. C., Dang, D., Song, B., et al. (2017). Controlled synthesis of three-phase Ni_xS_y/rGO nanoflake electrodes for hybrid supercapacitors with high energy and power density. *Nano Energy* 33, 522–531. doi: 10.1016/j.nanoen.2017.01.056

Dang, D., Zhao, B., Chen, D. C., Deglee, B., Qu, C., Dai, S. G., et al. (2018). A bi-functional WO_3-based anode enables both energy storage and conversion in an intermediate-temperature fuel cell. *Energy Storage Mater.* 12, 79–84. doi: 10.1016/j.ensm.2017.11.016

Du, J., Liu, L., Hu, Z. P., Yu, Y. F., Qin, Y. M., and Chen, A. B. (2018). Order mesoporous carbon spheres with precise tunable large pore size by encapsulated self-activation strategy. *Adv. Funct. Mater.* 28:1802332. doi: 10.1002/adfm.201802332

Fu, Y., Cai, X., Wu, H., Lv, Z., Hou, S., Peng, M., et al. (2012). Fiber supercapacitors utilizing pen ink for flexible/wearable energy storage. *Adv. Mater.* 24, 5713–5718. doi: 10.1002/adma.201202930

Guan, C., Liu, J., Wang, Y., Mao, L., Fan, Z., Shen, Z., et al. (2015). Iron oxide-decorated carbon for supercapacitor anodes with ultrahigh energy density and outstanding cycling stability. *ACS Nano* 9, 5198–5207. doi: 10.1021/acsnano.5b00582

Guo, X. L., Li, G., Kuang, M., Yu, L., and Zhang, Y. X. (2016). Tailoring kirkendall effect of the KCu_7S_4 microwires towards CuO@MnO_2 core-shell nanostructures for supercapacitors. *Electrochim. Acta* 174, 87–92. doi: 10.1016/j.electacta.2015.05.157

Hu, Z., Xiao, X., Chen, C., Li, T., Huang, L., Zhang, C., et al. (2015). Al-doped α-MnO_2 for high mass-loading pseudocapacitor with excellent cycling stability. *Nano Energy* 11, 226–234. doi: 10.1016/j.nanoen.2014.10.015

Hwu, S., He, L., Mackay, R., Kuo, Y., Skove, M., Mahapatro, M., et al. (1998). Bench-top synthesis of solid-state copper(I) sulfides, $KCu_{7-x}S_4$(x=0.0,0.12,0.34), via nonaqueous

electrochemistry. *Chem. Mater.* 10, 6–9. doi: 10.1021/cm9705395

Javed, M. S., Dai, S., Wang, M., Guo, D., Chen, L., Wang, X., et al. (2015). High performance solid state flexible supercapacitor based on molybdenum sulfide hierarchical nanospheres. *J. Power Sources* 285, 63–69. doi: 10.1016/j.jpowsour.2015.03.079

Jiang, Z. M., Xu, T. T., Yan, C. C., Ma, C. Y., and Dai, S. G. (2018). Urchin-like $Ni_{2/3}Co_{1/3}(CO_3)_{1/2}(OH)\cdot 0.11H_2O$ for high-performance supercapacitors. *Front. Chem.* 6:431. doi: 10.3389/fchem.2018.00431

Kim, S. K., Jung, E., Goodman, M. D., Schweizer, K. S., Tatsuda, N., Yano, K., et al. (2015). Self-assembly of monodisperse starburst carbon spheres into hierarchically organized nanostructured supercapacitor electrodes. *ACS Appl. Mater. Inter.* 7, 9128–9133. doi: 10.1021/acsami.5b01147

Li, M., Xu, W., Wang, W., Liu, Y., Cui, B., and Guo, X. (2014). Facile synthesis of specific $FeMnO_3$ hollow sphere/graphene composites and their superior electrochemical energy storage performances for supercapacitor. *J. Power Sources* 248, 465–473. doi: 10.1016/j.jpowsour.2013.09.075

Liu, C., Li, F., Ma, L. P., and Cheng, H. M. (2010). Advanced materials for energy Storage. *Adv. Mater.* 22, E28–62. doi: 10.1002/adma.200903328

Liu, M. Y., Niu, J., Zhang, Z. P., Dou, M. L., and Wang, F. (2018). Potassium compound-assistant synthesis of multi-heteroatom doped ultrathin porous carbon nanosheets for high performance supercapacitors. *Nano Energy* 51, 366–372. doi: 10.1016/j.nanoen.2018.06.037

Liu, W., Lu, C., Wang, X., Tay, R. Y., and Tay, B. K. (2015). High-performance microsupercapacitors based on two-dimensional graphene/manganese dioxide/silver nanowire ternary hybrid film. *ACS Nano* 9, 1528–1542. doi: 10.1021/nn5060442

Lu, X., Zeng, Y., Yu, M., Zhai, T., Liang, C., Xie, S., et al. (2014). Oxygen-deficient hematite nanorods as high-performance and novel negative electrodes for flexible asymmetric supercapacitors. *Adv. Mater.* 26, 3148–3155. doi: 10.1002/adma.201305851

Lu, X., Zhai, T., Zhang, X., Shen, Y., Yuan, L., Hu, B., et al. (2012). WO_{3-x}@Au@MnO_2 core-shell nanowires on carbon fabric for high-performance flexible supercapacitors. *Adv. Mater.* 24, 938–944. doi: 10.1002/adma.201104113

Niu, J., Shao, R., Liang, J. J., Dou, M. L., Li, Z. L., Huang, Y. Q., et al. (2017). Biomass-derived mesopore-dominant porous carbons with large specific surface area and high defect density as high performance electrode materials for Li-ion batteries and supercapacitors. *Nano Energy* 36, 322–330. doi: 10.1016/j.nanoen.2017.04.042

Niu, Z., Dong, H., Zhu, B., Li, J., Hng, H. H., Zhou, W., et al. (2013). Highly stretchable, integrated supercapacitors based on single-walled carbon nanotube films with continuous reticulate architecture. *Adv. Mater.* 25, 1058–1064. doi: 10.1002/adma.201204003

Park, D. H., Lee, S., Kim, T. W., Lim, S. T., Hwang, S., Yoon, Y. S., et al. (2007). Non-hydrothermal synthesis of ID nanostructured manganese-based oxides: effect of cation substitution on the electrochemical performance of nanowires. *Adv. Funct. Mater.* 17, 2949–2956. doi: 10.1002/adfm.200601126

Qu, C., Liang, Z. B., Jiao, Y., Zhao, B., Zhu, B. J., Dang, D., et al. (2018b). "One-for-All" strategy in fast energy storage: production of pillared MOF nanorod-templated positive/negative electrodes for the application of high-performance hybrid supercapacitor. *Small* 14:1800285. doi: 10.1002/smll.201800285

Qu, C., Zhang, L., Meng, W., Liang, Z. B., Zhu, B. J., Dang, D., et al. (2018a). MOF-derived a-NiS nanorods on graphene as an electrode for high-energy-density supercapacitors. *J. Mater. Chem. A* 6, 4003–4012. doi: 10.1039/c7ta11100b

Qu, C., Zhao, B., Jiao, Y., Chen, D. C., Dai, S. G., Deglee, B. D., et al. (2017). Functionalized bimetallic hydroxides derived from metal-organic frameworks for high-performance hybrid supercapacitor with exceptional cycling stability. *ACS Energy Lett.* 2, 1263–1269. doi: 10.1021/acsenergylett.7b00265

Reddy, A. L., Shaijumon, M. M., Gowda, S. R., and Ajayan, P. M. (2009). Coaxial MnO_2/carbon nanotube array electrodes for high-performance lithium batteries. *Nano Lett.* 9, 1002–1006. doi: 10.1021/nl803081j

Sankar, K. V., and Selvan, R. K. (2015). The ternary $MnFe_2O_4$/graphene/polyaniline hybrid composite as negative electrode for supercapacitors. *J. Power Sources* 275, 399–407. doi: 10.1016/j.jpowsour.2014.10.183

Shu, K., Wang, C., Li, S., Zhao, C., Yang, Y., Liu, H., et al. (2015). Flexible free-standing graphene paper with interconnected porous structure for energy storage. *J. Mater. Chem. A* 3, 4428–4434. doi: 10.1039/c4ta04324c

Simon, P., Gogotsi, Y., and Dunn, B. (2014). Where do batteries end and supercapacitors begin? *Science* 343, 1210–1211. doi: 10.1126/science.1249625

Sun, M., Wang, G., Yang, C., Jiang, H., and Li, C. (2015). A graphene/carbon nanotube@π-conjugated polymer nanocomposite for high-performance organic supercapacitor electrodes. *J. Mater. Chem. A* 7, 38880–33890. doi: 10.1039/c4ta06728b

Wang, M., Sun, L., Lin, Z., Cai, J., Xie, K., and Lin, C. (2013). p-n Heterojunction photoelectrodes composed of Cu_2O-loaded TiO_2 nanotube arrays with enhanced photoelectrochemical and photoelectrocatalytic activities. *Energ. Environ. Sci.* 6, 1211–1220. doi: 10.1039/c3ee24162a

Wang, M. J., Song, X. F., Dai, S. G., Xu, W. N., Yang, Q.i., Liu, J. L., et al. (2016). NiO nanoparticles supported on graphene 3D network current collector for high-performance electrochemical energy storage. *Electrochimica Acta* 214, 68–75. doi: 10.1016/j.electacta.2016.08.036

Wang, R., Yan, X., Lang, J., Zheng, Z., and Zhang, P. (2014b). A hybrid supercapacitor based on flower-like $Co(OH)_2$ and urchin-like VN electrode materials. *J. Mater. Chem. A* 2, 12724–12732. doi: 10.1039/c4ta01296h

Wang, X., Liu, B., Liu, R., Wang, Q., Hou, X., Chen, D., et al. (2014c). Fiber-based flexible all-solid-state asymmetric supercapacitors for integrated photodetecting system. *Angew. Chem. Int. Edit.* 53, 1849–1853. doi: 10.1002/anie.201307581

Wang, Y., Wang, Y., Jia, D., Peng, Z., Xia, Y., and Zheng, G. (2014a). All-nanowire based Li-ion full cells using homologous Mn_2O_3 and $LiMn_2O_4$. *Nano Lett.* 14, 1080–1084. doi: 10.1021/nl4047834

Xia, W., Qu, C., Liang, Z., Zhao, B., Dai, S., Qiu, B., et al. (2017). High-performance energy storage and conversion materials derived from a single metal–organic framework/graphene aerogel composite. *Nano Lett.* 17, 2788–2795. doi: 10.1021/acs.nanolett.6b05004

Xia, X., Zhang, Y., Chao, D., Guan, C., Zhang, Y., Li, L., et al. (2014). Solution synthesis of metal oxides for electrochemical energy storage applications. *Nanoscale* 6, 5008–5048. doi: 10.1039/c4nr00024b

Xu, J. M., Tang, H. B., Xu, T. T., Wu, D., Shi, Z. F., and Tian, Y. T. (2017). Porous NiO hollow quasi-nanospheres derived from a new metal-organic framework template as high-performance anode materials for lithium ion batteries. *Ionics* 23, 3273–3280. doi: 10.1007/s11581-017-2160-4

Xue, M., Xie, Z., Zhang, L., Ma, X., Wu, X., Guo, Y., et al. (2011). Microfluidic etching for fabrication of flexible and all-solid-state micro supercapacitor based on MnO_2 nanoparticles. *Nanoscale* 3, 2703–2708. doi: 10.1039/c0nr00990c

Yang, P., Chen, Y., Yu, X., Qiang, P., Wang, K., Cai, X., et al. (2014a). Reciprocal alternate deposition strategy using metal oxide/carbon nanotube for positive and negative electrodes of high-performance supercapacitors. *Nano Energy* 10, 108–116. doi: 10.1016/j.nanoen.2014.08.018

Yang, P., Li, Y., Lin, Z., Ding, Y., Yue, S., Wong, C. P., et al. (2014b). Worm-like amorphous MnO_2 nanowires grown on textiles for high-performance flexible supercapacitors. *J. Mater. Chem. A* 2, 595–599. doi: 10.1039/c3ta14275b

Yuan, L., Lu, X. H., Xiao, X., Zhai, T., Dai, J., Zhang, F., et al. (2012). Flexible solid-state supercapacitors based on carbon nanoparticles/MnO_2 nanorods hybrid structure. *ACS Nano* 6, 656–661. doi: 10.1021/nn2041279

Yuan, L., Yao, B., Hu, B., Huo, K., Chen, W., and Zhou, J. (2013). Polypyrrole-coated paper for flexible solid-state energy storage. *Energ. Environ. Sci.* 6, 470–476. doi: 10.1039/c2ee23977a

Zhang, Q. B., Chen, H. X., Luo, L. L., Zhao, B., Luo, H., Han, X., et al. (2018a). Harnessing the concurrent reaction dynamics in active Si and Ge to achieve high performance lithium-ion batteries. *Energy Environ. Sci.* 11, 669–681. doi: 10.1039/c8ee00239h

Zhang, Q. B., Liu, Z. C., Zhao, B., Cheng, Y., Zhang, L., Wu,. H. H., et al. (2018b). Design and understanding of dendritic mixed-metal hydroxide

nanosheets@N-doped carbon nanotube array electrode for highperformance asymmetric supercapacitors. *Energy Storage Mater*. doi: 10.1016/j.ensm.2018.06.026

Zheng, Z. M., Wu, H. H., Chen, H. X., Cheng, Y., Zhang, Q. B., Xie, Q. S., et al. (2018b). Fabrication and understanding of Cu_3SiSi@carbon@graphene nanocomposites as highperformance anodes for lithium-ion batteries. *Nanoscale* doi: 10.1039/c8nr07207h. [Epub ahead of print].

Zheng, Z. M., Zao, Y., Zhang, Q. B., Cheng, Y., Chen, H. X., Zhang, K. L., et al. (2018a). Robust erythrocyte-like Fe_2O_3@carbon with yolk-shell structures as highperformance anode for lithium ion batteries. *Chem. Eng. J.* 347, 563–573. doi: 10.1016/j.cej.2018.04.119

Conflict of Interest Statement: The authors declare that the research was conducted in the absence of any commercial or financial relationships that could be construed as a potential conflict of interest.